# Application of the Full Spectrum Correlated-*k* Distribution Approach to Modeling Non-Gray Radiation in Combustion Gases

**SANDIP MAZUMDER***
*CFD Research Corporation, Huntsville, AL 35805, USA*

**and**

**MICHAEL F. MODEST**
*Department of Mechanical and Nuclear Engineering, The Pennsylvania State University, University Park, PA 16802, USA*

The treatment of radiative transport through combustion gases is rendered extremely difficult by the strong spectral variation of the absorption coefficients of molecular gases. In the full spectrum correlated-*k* distribution (FSCK) approach, a transformation is invoked, whereby the radiative transfer equation (RTE) is transformed from wavenumber to non-dimensional Planck-weighted wavenumber space after reordering of the spectrum. The reordering results in a relatively smooth spectrum, allowing accurate spectral integration with very few quadrature points. The numerical procedures, required to use the FSCK model for full-scale combustion applications, have been outlined in this article. The FSCK model was first coupled with the Discrete Ordinates Method (DOM) for solution of the transformed RTE. The accuracy of the model was then examined for a variety of cases ranging from homogeneous one-dimensional media to inhomogeneous multi-dimensional media with simultaneous variations in both temperature and concentrations. Comparison with line-by-line calculations shows that the FSCK model is exact for homogeneous media, and that its accuracy in inhomogeneous media is limited by the accuracy of the scaling approximation. Several approaches for effective scaling of the absorption coefficient are examined. The model is finally used for radiation calculations in a full-scale combustor, with full coupling to fluid flow, heat transfer and multi-species chemistry. The computational savings resulting from use of the FSCK model is found to be more than four orders of magnitude when compared with line-by-line calculations. 

## NOMENCLATURE

| | |
|---|---|
| $a$ | base function (Eq. 22) |
| $f$ | absorption coefficient distribution function (Eq. 2) |
| $g,g_0$ | nondimensional Planck-weighted wavenumber |
| $i$ | partial Planck function (Eq. 15) |
| $I$ | radiation intensity ($W/m^2/sr$) |
| $I_b$ | Planck function ($W/m^2/sr$) |
| $k$ | recordered absorption coefficient ($m^{-1}$ or $m^{-1}$ $bar^{-1}$) |
| $L_m$ | mean beam length (m) |
| $s$ | path length (m) |
| $T$ | temperature (K) |
| $u$ | scaling function |
| $V$ | volume ($m^3$) |

### Greek

| | |
|---|---|
| $\alpha$ | absorbtivity |
| $\eta$ | wavenumber ($m^{-1}$) |
| $\kappa$ | absorption coefficient, linear or pressure based ($m^{-1}$ or $m^{-1}$ $bar^{-1}$) |
| $\kappa_p$ | Planck-mean absorption coefficient, linear or pressure based ($m^{-1}$ or $m^{-1}$ $bar^{-1}$) |
| $\sigma_s$ | scattering coefficient ($m^{-1}$) |
| $\tau$ | transmissivity |

### Subscripts

| | |
|---|---|
| *ref* | global reference value |
| $W$ | wall (or boundary) |

## INTRODUCTION

Radiation is one of the dominant modes of heat transfer in most combustion and fire applica-

* Corresponding author. E-mail: sm@cfdrc.com

0010-2180/02/$–see front matter
PII S0010-2180(02)00359-0

*COMBUSTION AND FLAME* 129:416–438 (2002)

Published by Elsevier Science Inc.

tions. With an increasing trend towards cleaner combustion (lean combustion with little soot), accurate prediction of radiation from molecular gases is beginning to occupy a position of central importance in the design of gas-fired combustion appliances. Radiative heat transfer in combustion gases is rendered extremely complex because of the line structure exhibited by the emission and absorption spectra of most combustion gases. Typical absorption spectra of gases such as $CO_2$, $H_2O$, and CO contain roughly $10^5$ to $10^6$ lines [1–3]. At combustion temperatures ($> 2000$ K), the number of lines present are well over a million [4, 5]. From a modeling perspective, this implies that to accurately predict radiative transport in flames, one would have to solve the radiative transfer equation (RTE) for a million or so spectral intervals. Such computations are referred to as line-by-line (LBL) calculations, and require extraordinarily large amounts of computer memory and time. The applicability of LBL computations [6–11] is currently limited to extremely simple geometries, specifically designed for validation of reduced models only. For combustion applications, where there are several additional key issues to deal with (including turbulence and chemical reactions), radiation is only one small piece of the gigantic puzzle, and it is impractical spending bulk of the computational time in performing LBL calculations. Despite tremendous advances in computer technology, judging by the time required for LBL calculations in simple one-dimensional gas layers, it is fair to say that such calculations will not be feasible for three-dimensional combustor geometries in the foreseeable future, and approximate models are necessary.

Approximate non-gray models, used to date, are based on spectral averaging either over many lines contained within a vibration-rotation band (wide-band models [3]), or over relatively fewer lines (narrow-band models [1, 12, 13]). This averaging is necessary to reduce the number of spectral intervals for which the RTE has to be solved. Spectral averaging results in an expression for the band emissivity and/or absorptivity, commonly referred to as the "band model." These band models make use of simple statistical relations based on the mean absorption line-strength and half-width distributions and require analytical integration of the RTE over small spectral intervals. The accuracy of such band models, even for homogeneous media, is largely determined by the narrowness of the bands, and the statistical models employed during analytic integration within the band. Wide-band models are known to be inaccurate for combustion applications, because of the inherent inaccuracy in treating the so-called "wings" of the band, which usually require spectral resolution much finer than a few tens of wavenumbers [14]. On the other hand, although narrow-band models can be sometimes quite fruitful, accurate modeling of radiation from a $CO_2$-$H_2O$ mixture at high temperature would require several hundreds of narrow-bands. Furthermore, there is no universally applicable proven statistical model available for narrow-band integration. On account of all these shortcomings, despite the existence of both narrow-band and wide-band models for more than three decades, there has been little success in modeling radiative transport in combustion gases.

In recent years, there has been a lot of activity in trying to model non-gray radiation in molecular gases using global approaches, as opposed to band models. The correlated-*k* (CK) method is based on the fact that inside a spectral interval, which is sufficiently narrow to assume a constant Planck function, the precise position of a spectral line is unimportant for spectral integration. If the medium is homogeneous or the absorption coefficient obeys the so-called scaling approximation, the absorption coefficient can be reordered into a smooth monotonically increasing function. Because of the presence of "hot lines," the CK method is known to give poor accuracy in cases with extreme temperature variation. For such scenarios, Riviere and co-workers [10, 15, 16] developed the so-called correlated-*k* fictitious gas model. Starting with a high-resolution database, they grouped lines according to the values of their lower energy level and found the *k*-distribution for each of the fictitious gases, making the CK method more accurate when applied to each fictitious gas separately than when applied to the real gas. They further assumed that the positions of lines belonging to different classes are statistically uncorrelated. Unfortunately, the method only

supplies the mean transmissivity for a gas layer, that is, it loses the most important advantages of using *k*-distributions, limiting its application to nonscattering media within black enclosures.

Modest and Zhang [9] have demonstrated, based on analysis, that the CK method is, in essence, a close relative of the weighted-sum-of-gray gases (WSGG) method [17]. Denison and Webb [7, 8, 18, 20] have improved considerably on the WSGG method by developing a spectral-line-weighted (SLW) WSGG model based on detailed spectral line data. They also extended the SLW model to inhomogeneous media by introducing a cumulative distribution function of the absorption coefficient, calculated over the whole spectrum and weighted by the Planck function [21]. The method developed by the French researchers [10, 11] is almost identical to the SLW model, and differs only in the way the fictitious gas weights are calculated. These weights are chosen in such a manner that emission by an isothermal gas column is predicted exactly. Pierrot et al. [11] developed a global fictitious gas model to improve the treatment for strongly inhomogeneous media. The ideas used to develop the full spectrum correlated-*k* distribution (FSCK) model are derived, in part, from the work of Webb and co-workers and the French group.

In this work, the FSCK model has been validated extensively for multidimensional geometry with combined temperature and concentration discontinuities. Several different scaling techniques have been examined to determine which of these is the most accurate. Finally, the model has been used for radiation calculations in a full-scale combustor with full coupling to the conservation equations for mass, momentum, energy, and species. The article advances the state of the art by demonstrating the feasibility of using the FSCK model for full-scale calculation of radiative transport in combustion systems.

## THEORY

### Spectral Reordering and *k*-distribution

Consider a participating molecular gas bounded within a black-walled enclosure. In such a situation, the spectral intensity at any point within the gas depends on the temperature (through the Planck function) and the spectral absorption coefficient of the gas. Over a small spectral interval (so-called "narrow-band"), such as a few tens of wavenumbers, the Planck function is essentially constant. Thus, across such a small spectral interval, the spectral intensity is a function of the absorption co-efficient only. Figure 1 shows the absorption coefficient of $CO_2$ across a very small part of its 4.3 $\mu$m band. It is clear from this figure that the absorption coefficient varies strongly even within such a narrow spectral interval. It attains the same value several times within the same spectral interval, each time producing an identical spectral intensity field within the medium. This implies that line-by-line calculations of the radiation intensity would be wasteful, because the same calculations would be performed several times. If the absorption coefficient can be somehow reordered such that the intensity calculations are performed only once for each absorption coefficient value, the resulting computations would be immensely more efficient without sacrificing the accuracy. Although this reordering concept was first reported in the western literature about three decades ago by Arking and Grossman [22], it has received significant attention within the atmospheric science and heat transfer communities only in the last decade or so [6, 14, 23, 24].

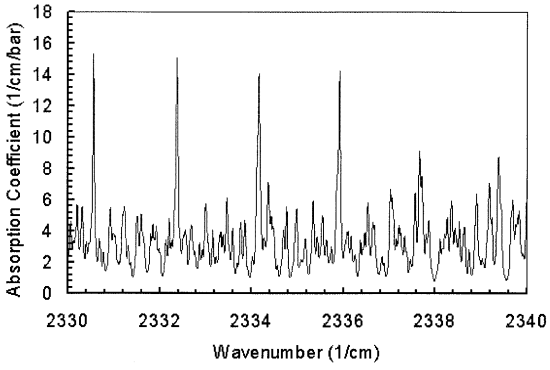


Fig. 1. Pressure-based absorption coefficient of a small part of the $CO_2$ 4.3 $\mu$m band at 1500K computed using the HITEMP database [5].

The narrow-band transmissivity (i.e., spectral average over a narrow-band) of a homogeneous gas layer of width $X$, is written as:

$$\overline{\tau_\eta}(X) = \frac{1}{\Delta\eta}\int_{\Delta\eta} e^{-k_\eta X} d\eta \tag{1}$$

Let us now define a function $f(k)$, such that

$$f(k) = \frac{1}{\Delta\eta}\int_{\Delta\eta} \delta(k - \kappa_\eta) d\eta \tag{2}$$

where $\delta(k - \kappa_\eta)$ is the Dirac-delta function. Substituting Eq. 2 into Eq. 1, the narrow-band transmissivity may be re-written as:

$$\overline{\tau_\eta}(X) = \int_0^\infty e^{-kX} f(k) dk \tag{3}$$

Noting that, in the vicinity of each point where $\kappa_\eta = k$, we can replace $d\eta$ by $(d\eta/d\kappa_\eta)d\eta$, the integration in Eq. 2 over $\Delta\eta$ gives a weighted sum of the number of points where $\kappa_\eta = k$ [6]:

$$f(k) = \frac{1}{\Delta\eta}\sum_i \left|\frac{d\eta}{d\kappa_\eta}\right|_i \tag{4}$$

From Eq. 4, it is clear that for every maximum or minimum of the absorption coefficient $\kappa_\eta$, the function $f(k)$ will assume a value of infinity, because $d\kappa_\eta/d\eta = 0$. This implies that using Eq. 3 for integration is numerically not amenable. The problem can be circumvented by using the integral of $f(k)$, which happens to be a smooth function. Equation 3 can then be written as:

$$\overline{\tau_\eta}(X) = \int_0^\infty e^{-kX} f(k) dk = \int_0^1 e^{-k(g)X} dg \tag{5}$$

where the so-called *cumulative distribution function* $g(k)$ is defined as [6]:

$$g(k) = \int_0^k f(k') dk' \tag{6}$$

It is evident from Eq. 5 that computation of the transmissivity requires evaluation of $k(g)$. The function $k(g)$ is commonly referred to as the $k$-distribution, and is obtained by numerical inversion of Eq. 6. Algorithms for numerical evaluation of the $k$-distribution will be discussed in sections to follow.

## FSCK Model

The above arguments for reordering hold only if the Planck function does not vary within the spectral interval in question. While this is a very good assumption within a narrow band, it is invalid for a spectral interval larger than a few tens of wavenumbers. The evaluation of overall radiative heat fluxes, however, requires spectral integration over the whole spectrum. Although savings can be achieved by employing $k$-distributions within every narrow-band for spectral integration, extending this concept in its original form to the full spectrum would still require thousands of quadrature points and prohibitively large computational resources. The challenge is to reorder the absorption coefficient of the entire spectrum once and for all by accounting for the Planck function variation across the spectrum, as well. The FSCK model overcomes this challenge. The theory underlying this model is described here briefly to facilitate discussion of numerical algorithms and results. Further details pertaining to this model may be obtained from the articles by Modest and co-workers [9, 25].

Consider a participating gas within a black enclosure. For simplicity in mathematical derivation, we will assume that the medium only absorbs and emits, and does not scatter. It will be shown later that the model is equally accurate for gray scattering media with gray walls. The RTE, under these assumptions, is given by [26]:

$$\frac{dI_\eta}{ds} = \kappa_\eta(I_{b\eta} - I_\eta) \tag{7}$$

where $I_\eta$ is the spectral intensity varying along a path $s$, $\eta$ is the wavenumber, $I_{b\eta}$ is the Planck function, and $\kappa_\eta$ is the spectral absorption coefficient. The spectral absorption coefficient, $\kappa_\eta$, is a function (besides $\eta$) of temperature, pressure, and species concentrations. The formal solution of Eq. 7 is [26]:

$$I_\eta(s) = I_{bw\eta} \exp\left(-\int_0^s \kappa_\eta ds''\right) + \int_0^s I_{b\eta}(Ts')) \cdot \exp\left(-\int_{s'}^s \kappa_\eta ds''\right)\kappa_\eta(s')ds' \quad (8)$$

where $I_{bw\eta}$ denotes the Planck function evaluated at the wall temperature. Integrated over the whole spectrum, Eq. 8 becomes

$$I(S) = \int_0^\infty I_\eta d\eta = I_{bw}[1 - \alpha(T_w, 0 \to S)] + \int_0^s I_b(s')\frac{\partial \alpha}{\partial s'}(T(s'), s' \to s)ds' \quad (9)$$

where

$$\alpha(T, s' \to s) = \frac{1}{I_b(T)}\int_0^\infty I_{b\eta}(T) \cdot \left[1 - \exp\left(-\int_{s'}^s \kappa_\eta ds''\right)\right]d\eta \quad (10)$$

At this point, it is convenient to introduce the so-called scaling approximation [26]:

$$\kappa_\eta(\eta, T, p_i) = k_\eta(\eta)u(T, p_i) \quad (11)$$

which states that the wavenumber dependence of the absorption coefficient is unique and does not depend on temperature and partial pressure. While being a good assumption for soot, it is not valid for molecular gas mixtures in general. The accuracy of this approximation will be evaluated and discussed thoroughly for a major part of this article, as it constitutes a very important aspect of modeling radiation in inhomogeneous paths. Substitution of Eq. 11 into Eqs. 8 and 10 yields:

$$I_\eta(s) = I_{bw\eta}e^{-k_\eta X(0,s)} + \int_0^s I_{b\eta}(s')e^{-k_\eta X(s',s)}k_\eta u(s')ds' \quad (12)$$

and

$$\alpha(T, s' \to s) = \frac{1}{I_b(T)}\int_0^\infty I_{b\eta}(T)[1 - e^{-k_\eta X(s',s)}]d\eta \quad (13)$$

where

$$X(s', s) = \int_s^s u(s'')ds'' \quad (14)$$

A similar reordering argument can now be applied to the entire spectrum. Defining a fractional Planck function as

$$i(T, \eta) = \frac{1}{I_b(T)}\int_0^\eta I_{b\eta}(\eta')d\eta' \quad (15)$$

it is obvious that $i(T,0) = 0$ and $i(T, \infty) = 1$, and that the fractional Planck function increases monotonically from 0 to 1. Furthermore, there is a single value of $k_\eta$ for each value of $i$, but many values of $i$ for each value of $k_\eta$. Thus, Eq. 1 can be reordered the same way as Eq. 5 to yield:

$$\tau = \int_0^1 e^{-k_\eta(i)X}di = \int_0^\infty e^{-kX}f(T,k)dk = \int_0^1 e^{-k(T,\,g)X}dg \quad (16)$$

where $\tau$ is the overall transmittance (including all wavenumbers). *It is very important to note here that g is no longer an equivalent wavenumber, but an equivalent Planck-weighted wavenumber.* Because $i$ is a function of $T$, so is $k$, such that $k = k(T, g)$. The goal in using the reordering approach is to transform the RTE in such a way that a reordered absorption coefficient of the form $k = k(g)$ can be used instead of $\kappa = \kappa(\eta)$. Thus, the fact that $k$ is now a function of both $T$ and $g$, is inconvenient to implement for arbitrary solution techniques of the RTE. To circumvent

this problem, following Modest [17], an additional reordering step is performed, such that:

$$\tau = \int_0^1 e^{-k(T,g)X} dg = \int_0^1 a(T,g_0) e^{-k(T_0,g_0)X} dg_0 \tag{17}$$

where $k = k(T_0, g_0)$ is the $k$-distribution evaluated at $T = T_0$. In other words, the temperature dependence of $k$ has been moved to the base function $a$. Setting $k(T, g) = k(T_0, g_0)$, and differentiating leads to

$$dg = \frac{\partial k(T_0,g_0)/\partial g_0}{\partial k(T,g)/\partial g} dg_0 = \frac{f(T,k(g))}{f(T_0,k(g_0))} dg_0 = a(T,g_0) dg_0 \tag{18}$$

where $a(T_0, g_0)$ has been set to unity at the reference condition. For simplicity of notation, henceforth, the subscript "0" will be dropped from $g_0$. Also, $k(T_0, g_0)$ will simply be written as $k(g)$, with the understanding that $k(g)$ is the $k$-distribution evaluated at the reference state. Equation 17 can be differentiated to yield:

$$\frac{\partial \alpha}{\partial s'} = -\frac{\partial \tau}{\partial s'} = \int_0^1 a(T, g) e^{-k(g)X(s',s)} k(g) \frac{\partial X}{\partial s'} dg = -\int_0^1 a(T, g) e^{-k(g)X} k(g) u(s') dg \tag{19}$$

Substitution into Eq. 12 yields:

$$I(s) = \int_0^1 I_g(s) dg = \int_0^1 \left\{ [a(T_w,g) I_{bw}] e^{-kX(0,s)} + \int_0^s [a(T(s'),g) I_b(s')] e^{-kX(s',s)} k u(s') ds \right\} dg \tag{20}$$

Comparison of Eq. 20 with Eq. 9, we find that the integral form of the generalized RTE has been recovered, except that the Planck function has been replaced by a weighted Planck function $aI_b$. In differential form, the transformed RTE, with the inclusion of scattering, can be re-written as [9]:

$$\frac{dI_g}{ds} = k(g) u(s) (a I_b - I_g) - \sigma_s I_g + \frac{\sigma_s}{4\pi} \int_{4\pi} I_g(s') \Phi(s,s') d\Phi' \qquad \forall\, 0 \le g \le 1 \tag{21}$$

Equation 21 is our new transformed RTE and needs to be solved for several different $g$ values and finally integrated to obtain the overall radiative flux.

The treatment of soot is an important aspect of modeling radiation in combustion systems. The FSCK model does not preclude existence of soot particles. Modest and Zhang [9] have already demonstrated that the model is applicable to situations where soot is mixed with gas components. In combustion scenarios, prediction of soot volume fraction, particle size, and morphology is in itself a topic of current research. To perform radiation calculations with soot, such data is necessary, and this is beyond the scope of the current study.

### Computation of *k*-distributions, Base Functions, and Scaling Functions

Before solution of Eq. 21 it is necessary to compute $k(g)$, $u(s)$, and $a(T, g)$. This constitutes a major task in using the FSCK model for radiation calculations. The central idea is to generate databases for the three functions once and for all, and re-use this database for all problems of interest. This would imply that once the databases have been generated, the computational requirements would be limited to that for solving the RTE for a few quadrature points ($g$ values) only.

### *k*-distributions and Base Function

There are several numerical techniques to compute the $k$-distribution from raw line-by-line absorption coefficient data. For the current study, we employed an algorithm that is convenient and fast. The steps are outlined below.

- The raw absorption coefficient ($\kappa$ vs. $\eta$) is first read in from a file for a given temperature. This is the reference temperature. Additional nodes are then introduced in wavenumber space. For example, if the raw absorption coefficient is stored at intervals of 0.01 $cm^{-1}$, additional nodes may be introduced at intervals of 0.001$cm^{-1}$.
- The $\kappa$ values at these intermediate additional nodes are computed by linear interpolation. These are henceforth referred to as $\kappa$-samples.
- The $\kappa$ axis is then broken up into sampling bins (henceforth, referred to as $\kappa$-bins). The number of bins to be used is quite arbitrary. The smaller the number of bins, the smoother the resultant $k$-distribution will be. For the current study, 100 bins were taken for each decade of increase of $\kappa$.
- The spectrum is then scanned for all the $\kappa$-samples. Depending on which $\kappa$-bin the sample belongs to, the fractional Planck function is computed and cumulatively added to the bin value for every temperature. For the current study, temperature nodes were placed every 100 K starting from 300 K and going up to 2000 K.
- After all $\kappa$-samples have been scanned, the bin values for all temperatures are multiplied by $\pi/\sigma T_i^4$. At this point, the bin values represent $f\,(T, k_j)\Delta k_j$.
- The function $g(k)$ is next evaluated using: $g(T_i, k_j) = g\,(T_i, k_{j-1}) + f\,(T_i, k_j)\Delta\, k_j$.
- Of interest to us is $k$ versus $g$ rather than $g$ versus $k$. The function $g(T, k)$ is next inverted numerically by linear interpolation to get $k(T, g)$ at all temperature nodes, and stored at 1000 $g$-values.

Once $f(T, k_j)$ has been computed for all $T$, the base function $a(T, k_j)$ can easily be computed using

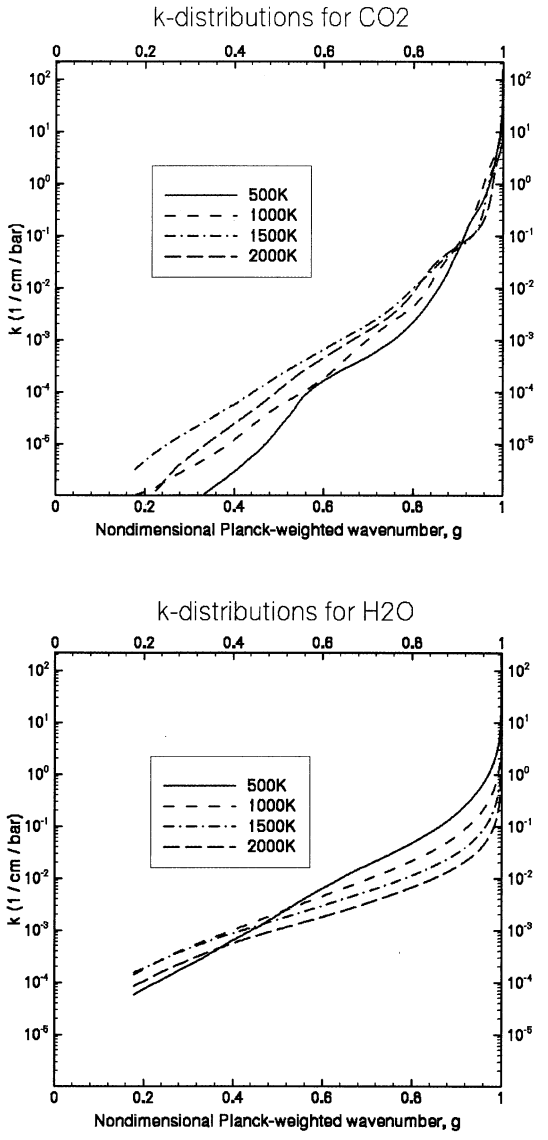


Fig. 2. $k$-distributions for $CO_2$ and $H_2O$ at different reference temperatures computed from the HITEMP database [5].

$$a(T,k_j) = \frac{f(T,k_j)}{f(T_0,k_j)} \tag{22}$$

Once again, the function is inverted numerically to obtain $a(T, g)$ versus $g$ at all $T$, and stored at 1000 $g$ values. Figure 2 shows $k$-distributions for $CO_2$ and $H_2O$ at different temperatures, computed using the above algorithm. It is clear from Fig. 2 that the function $k(g)$ is much smoother than $\kappa(\eta)$, shown in Fig.1. This implies that the integra-

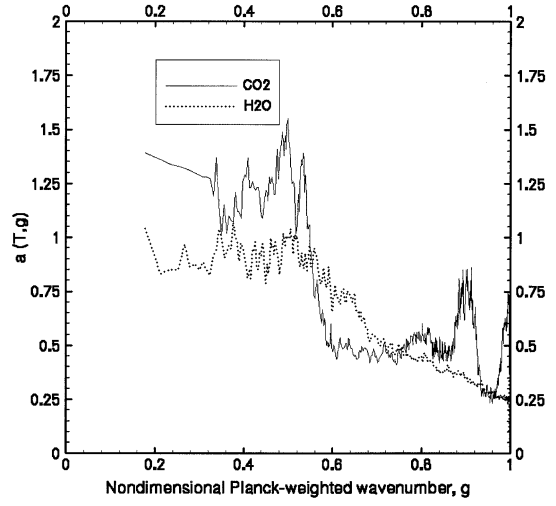


Fig. 3. Base function $a(T, g)$ cmputed using the HITEMP database for $CO_2$ and $H_2O$ at 2000K with a reference temperature of 500K.

tion over $g$-space in Eq. 20 would require very few quadrature points (typically less than 20) as opposed to the integration of Eq. 9, which would require millions of quadrature points. The computational benefits of using the FSCK model are, thus, unquestionable. Figure 3 shows the base function $a(T, g)$ for $CO_2$ and $H_2O$ at a reference temperature of 500 K. $a(T, g)$ is not as smooth as the $k$-distributions shown in Fig. 2, and high frequency oscillations are observed. Modest and Zhang [9] suggest smoothing of the base function to improve accuracy. For the current study, the smoothing was performed using least square spline fits to the data.

### Scaling Function

It is obvious from the above section that the scaling approximation, as described by Eq. 11, is necessary to reorder the absorption coefficient for the whole spectrum. This is not a restriction that has been imposed by the current FSCK model, but is, rather, an approximation that cannot be easily bypassed if one were to treat radiation through inhomogeneous paths. For example, the exact same scaling technique is applied in the popular Curtis-Godson scaling approximation to calculate narrow-band absorptivities for inhomogeneous paths [26]. While its use has been prolific, its accuracy is questionable, and requires further examination.

Determination of a scaled absorption coefficient from line-by-line data consists of two major steps. First, an appropriate reference temperature must be chosen, at which the absorption coefficient is set to coincide with that of the database, that is, $\kappa_\eta(\eta, T_{ref}, p_{i,ref}) = k_\eta(\eta)$ and $u(T_{ref}, p_{i,ref}) = 1$. Secondly, based on energy balance, a relationship between the scaling function, the local absorption coefficient, and the reference absorption coefficient needs to be developed. Because radiative heat fluxes from a gaseous layer are governed by emission rates attenuated by self-absorption, we evaluate the scaling function in this research from the relationship

$$\int_0^\infty I_{b\eta} T_{ref}) \exp[-\kappa_\eta(T, p_{i,ref}) L_m] d\eta = \int_0^\infty I_{b\eta}(T_{ref}) \exp[-k_\eta u(T, p_{i,ref}) L_m] d\eta \tag{23}$$

where $L_m$ is the mean beam length within the gas layer ($= 4V/A$). For optically thin situations, Eq. 23 ensures that the Planck mean absorption coefficient is recovered by scaling. For optically thick situations, Eq. 23 ensures that the scaling has the correct heat flux escaping a layer of thickness $L_m$. The mean beam length is problem dependent, and therefore, to enable use of a table for the scaling function, it is necessary to tabulate values at several different mean beam lengths, as well, in addition to several different reference temperatures, reference concentrations (or partial pressures) and local temperatures. For the current study, for each $T_{ref}$ and $p_{ji,ref}$, values of $u$ were tabulated for several $T$ values and $L_m$ values. The $T$ and $T_{ref}$ values were varied from 300 K to 2000 K, with intervals of 100 K. The $L_m$ values were varied from 1 cm to 10 m with 20 unequally spaced intermediate values. The reference mole fraction values were varied from 4% to 80% with 20 intermediate

values. Such high values of mole fraction were deemed necessary, because state-of-the-art combustion appliances are often fired with pure oxygen rather than air. From the above discussion, it is clear that Eq. 23 needs to be solved 129,600 times (18 $T_{ref}$ × 18 $T$ × 20 $p_{i,ref}$ × 20 $L_m$) for each gas in question. This is a formidable task in light of the fact that Eq. 23 is a non-linear equation in $u$, and iteration is necessary. Furthermore, because the absorption coefficient is stored at more than a million wavenumbers, the integral reduces to a summation over a million terms and is, thus, expensive to evaluate. For the present study, Eq. 23 was solved using the Newton-Raphson iterative procedure, with particular emphasis on making the initial guess very close to the actual solution. The solution of Eq. 23 required 8 s of CPU on a Pentium III 733 MHz processor for each case, implying that the calculation for all 129,600 cases required about 20 days of CPU for each gas. It must be emphasized here that once the scaling function has been tabulated for the whole range of reference temperature, reference partial pressure, local temperature, and mean beam length, it can be used for any problem. The solution of Eq. 23 is a one-time affair for each gas, and therein lies the advantage of the FSCK method. Figure 4 shows scaling functions for $CO_2$ and $H_2O$ for various local temperatures and mean beam lengths.

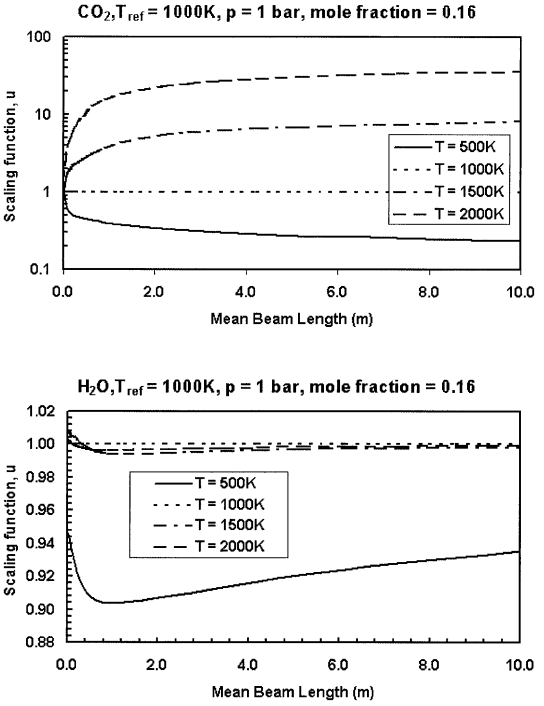


Fig. 4. Scaling functions for $CO_2$ and $H_2O$ computed using the HITEMP database [5].

It is evident from Eq. 23 that the scaling function will be dependent upon the reference temperature and concentrations used. The choice of an appropriate reference temperature and an appropriate reference concentration is a tricky matter and needs further investigation. In later sections, this issue will be evaluated and discussed comprehensively.

**Solution of the Transformed RTE**

Several different well-known techniques are available to solve the transformed RTE, (Eq. 21). These include the method of spherical harmonics ($P_N$ approximation [27]), the discrete ordinates method [28, 29], the discrete transfer method [30], and the Monte Carlo method [31]. Over the last decade or so, the discrete ordinates method (DOM) has become the RTE solver of choice for commercial CFD codes. A discussion of its strengths or weaknesses is beyond the scope of this article, and may be found elsewhere [28]. CFD Research Corporation's commercial software, CFD-ACE+, is already equipped with a DOM-based RTE solver for multi-dimensional geometry with arbitrary grid topology [32]. The model is fully coupled with the overall energy equation, and allows solution of the RTE for both gray and non-gray cases with spatially varying extinction coefficient. This model served as the starting point for implementation of the solution technique of the transformed RTE. The overall solution procedure is depicted schematically in Fig. 5. It is worth noting that the solution strategies depicted in Fig. 5 can be applied to any general-purpose flow solver. The solution algorithm also depicts that the database of $k$-distributions, base functions and scaling functions is a stand-alone piece, which is generated only once, and is used repeatedly for any possible application. The solution of Eq. 23, which happens to be computationally expensive, is a one-time affair only.

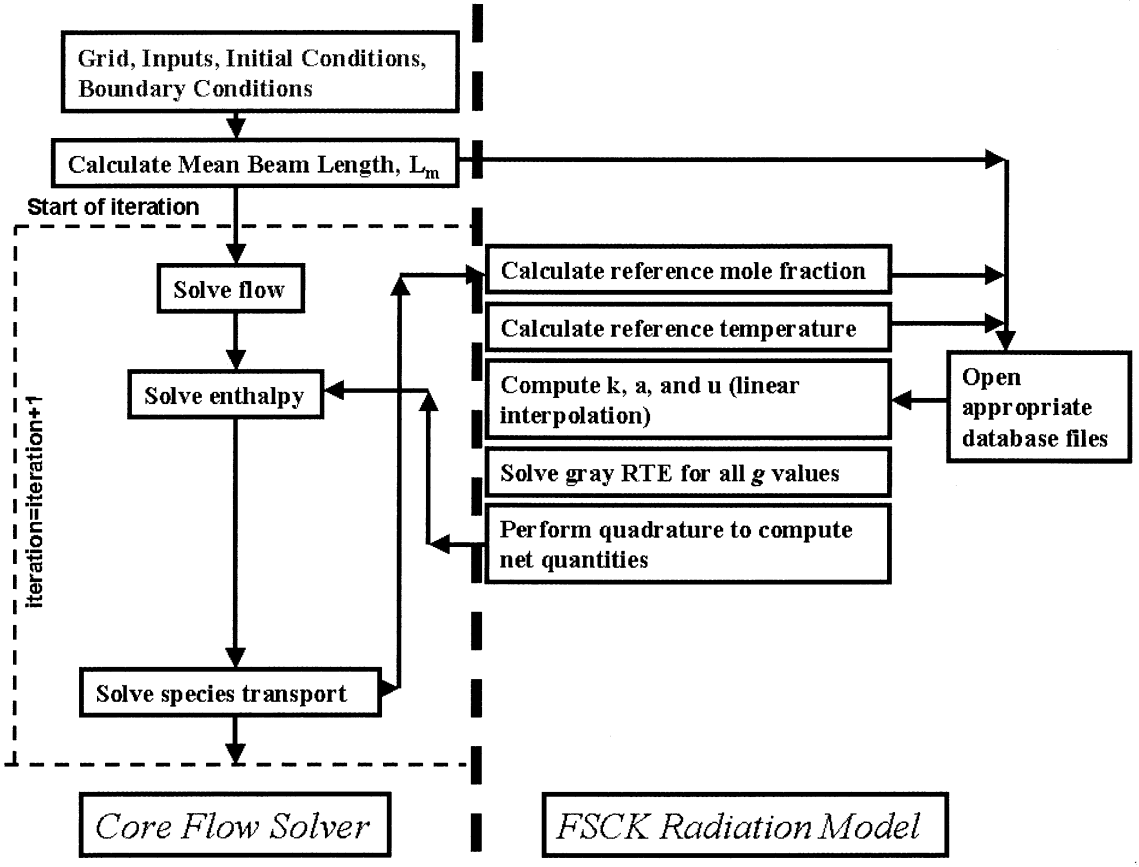


Fig. 5. Solution strategies employed to accommodate the FSCK model in the commercial CFD code, CFD-ACE+.

## RESULTS AND DISCUSSION

The FSCK model was verified and validated for a number of different scenarios ranging from homogeneous paths to inhomogeneous paths with simultaneous variation of both concentration and temperature fields. This section describes in detail each validation study that was performed, and the conclusions drawn from the results. All results presented in this section were obtained using the HITEMP database [5], which is a high-temperature rendition of the HITRAN96 spectroscopic database.

### Homogeneous Path

The only approximation introduced in development of the FSCK model is the scaling approximation. If the radiation path is homogeneous (i.e., the domain of interest has uniform temperature and/or concentration fields), the scaling approximation becomes mute, that is, the scaling function is equal to unity everywhere by definition. Under this circumstance, it is expected that the FSCK model will produce results, which match perfectly with exact LBL calculations.

To verify this matter, a simple problem was concocted. In this problem, a hot gas comprising of 10%$CO_2$ and 90%$N_2$ (assumed to be nonparticipating) at 1500 K was confined between two infinitely long parallel plates at 0K. The temperature and concentration fields were fixed and not allowed to change. The distance between the plate was a parameter, which was changed to vary the optical thickness of the medium.

The RTE can be solved analytically for this problem [26]. As a first step, our goal was to investigate the accuracy of the discrete ordinates method and other RTE solution techniques for this problem. To do so, we used the

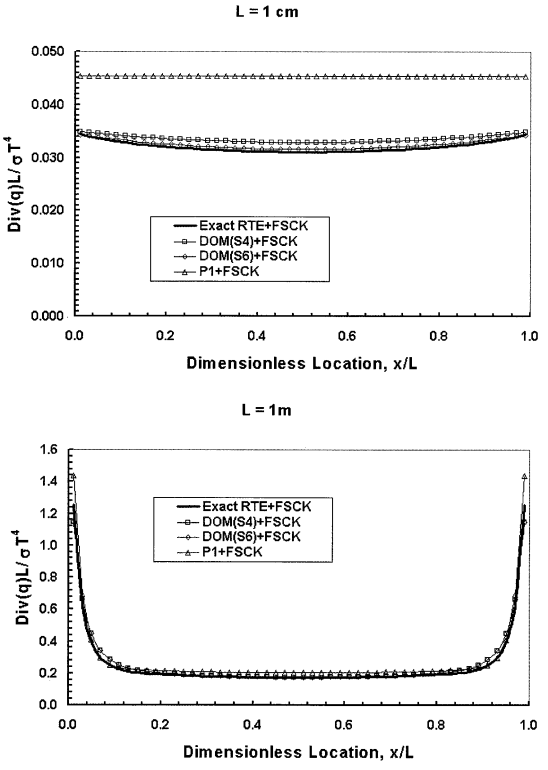


Fig. 6. Divergence of radiative heat flux computed using different solution techniques in conjunction with the FSCK model. $L$ is the gap between the two parallel plates.

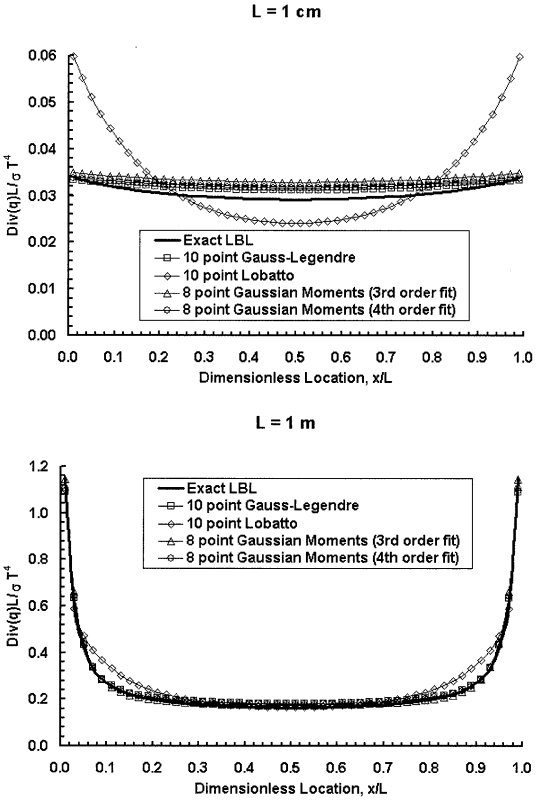


Fig. 7. Comparison of FSCK model with exact solution. "Exact LBL" represents analytical solution of the RTE in conjunction with line-by-line integration. The other four curves were computed using the FSCK model in conjunction with S4 DOM.

FSCK model in conjunction with exact analytical solution of the RTE, several variations of DOM, and the P-1 approximation. In each case a 10 point Gauss-Legendre quadrature [33] was employed for integration in $g$-space. The results are shown in Fig. 6 for two different optical thicknesses. As expected, the DOM S6 method produces the most accurate results, closely followed by the DOM S4 results. The P-1 method overpredicts the divergence significantly, especially for the lower optical thickness case.

Once it was determined that the discrete ordinates method is accurate for such computations, we proceeded to verify the accuracy of the FSCK model by comparison with exact line-by-line calculations. In the context of using the $k$-distribution approach for global heat transfer calculations, one question, which has been raised over the years by several researchers [9,11], is what quadrature scheme is most suited for integration over $g$-space. This is particularly critical for full-spectrum calculations, where we are replacing millions of spectral quadrature points by a few tens of points. Obviously, with such few points, the quadrature to be used is expected to affect the results of integration significantly. Literature review revealed that Gauss-Legendre qudrature schemes and Lobatto quadrature schemes were the two most widely used. Careful study of $k$-distributions (Fig. 2) revealed that $k$-distributions of all molecular gases tend of have a steep gradient close to $g = 1$. This implies that the quadrature points need to be clustered around $g = 1$ to produce accurate integration results. In light of these observations, we started experimenting with Gaussian Quadrature of Moments (GQM) schemes [33], and soon found that they are indeed very accurate for this type of application. Figure 7 shows comparison of the FSCK model with exact line-by-line calculations for the same

**TABLE 1**

Wall Heat Fluxes: Comparison Against Exact Solution. The Percentage Errors are Shown in Parentheses

| Model | Non-dimensional Wall Heat Flux | |
|---|---|---|
| | L = 1 cm | L = 1 m |
| Exact LBL | 0.0153 | 0.13338 |
| 10 point Gauss-Legendre | 0.01596 (4.3%) | 0.13547 (1.6%) |
| 10 point Lobatto | 0.01692 (10.6%) | 0.14313 (7.3%) |
| 8 point Gaussian Moment with 3rd order fit | 0.01677 (9.6%) | 0.13457 (0.9%) |
| 8 point Gaussian Moment with 4th order fit | 0.0162 (5.8%) | 0.13498 (1.2%) |

problem described earlier. The corresponding wall heat fluxes are tabulated in Table 1.

From Fig. 7, it is clear that the 8-point Gaussian quadrature of moments proved to be the most accurate integration scheme at least for this particular problem for both optical thickness. The 10-point Gauss-Legendre scheme was also found to be quite accurate, although it requires two extra points (20% more CPU). The Lobatto quadrature scheme was deemed unsatisfactory for the optically thinner case.

From the results presented above, it is clear that the FSCK model indeed produces almost exact answers. The small errors are attributed to differences between exact solutions and DOM, and errors because of interpolation and numerical integration using less than 10 points. The next task undertaken was to validate the model for inhomogeneous paths.

## Inhomogeneous Path

### Temperature Inhomogeneity

The first problem we studied is that of a gas of uniform concentration confined between infinitely large parallel plates, with a jump in temperature in the middle of the gas layer. This is shown schematically in Fig. 8. The cold and hot layer thicknesses were retained as parameters. Scattering was neglected and the walls were black. LBL (with S4-DOM) and FSCK calculations were performed for various cold layer thicknesses. Comparison of the radiative heat flux divergence is shown in Fig. 9. The corresponding heat fluxes are depicted in Fig. 10.

As discussed earlier, the scaling approximation plays a critical role in the accuracy of FSCK results. In particular, the choice of an appropriate reference temperature is important for producing accurate answers for inhomogeneous paths. Although the scenario described above appears to be rather benign on account of the simple geometry and boundary conditions, a temperature discontinuity of 1000 K is anything but benign in terms of scaling.

There are several approaches for fixing the reference temperature. Modest and Zhang [9] has suggested use of volume average of the fourth-power of temperature (denote in Figs. 9 and 10 as "VAT") defined as:

$$T_{ref}^4 = \frac{1}{V}\int_V T^4 dV \tag{24}$$

They also indicated [9] that the Planck-mean temperature (denoted by "PMT" in Figs. 9 and 10), defined by the implicit relationship

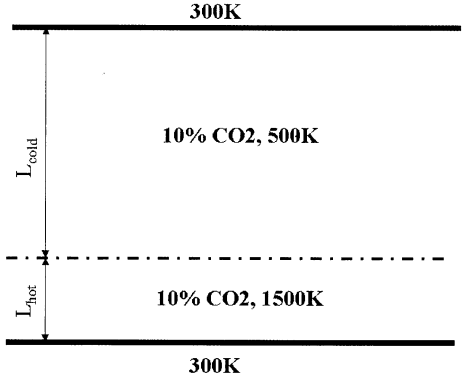


Fig. 8. Schematic of the 2-layer case used to validate the FSCK model.

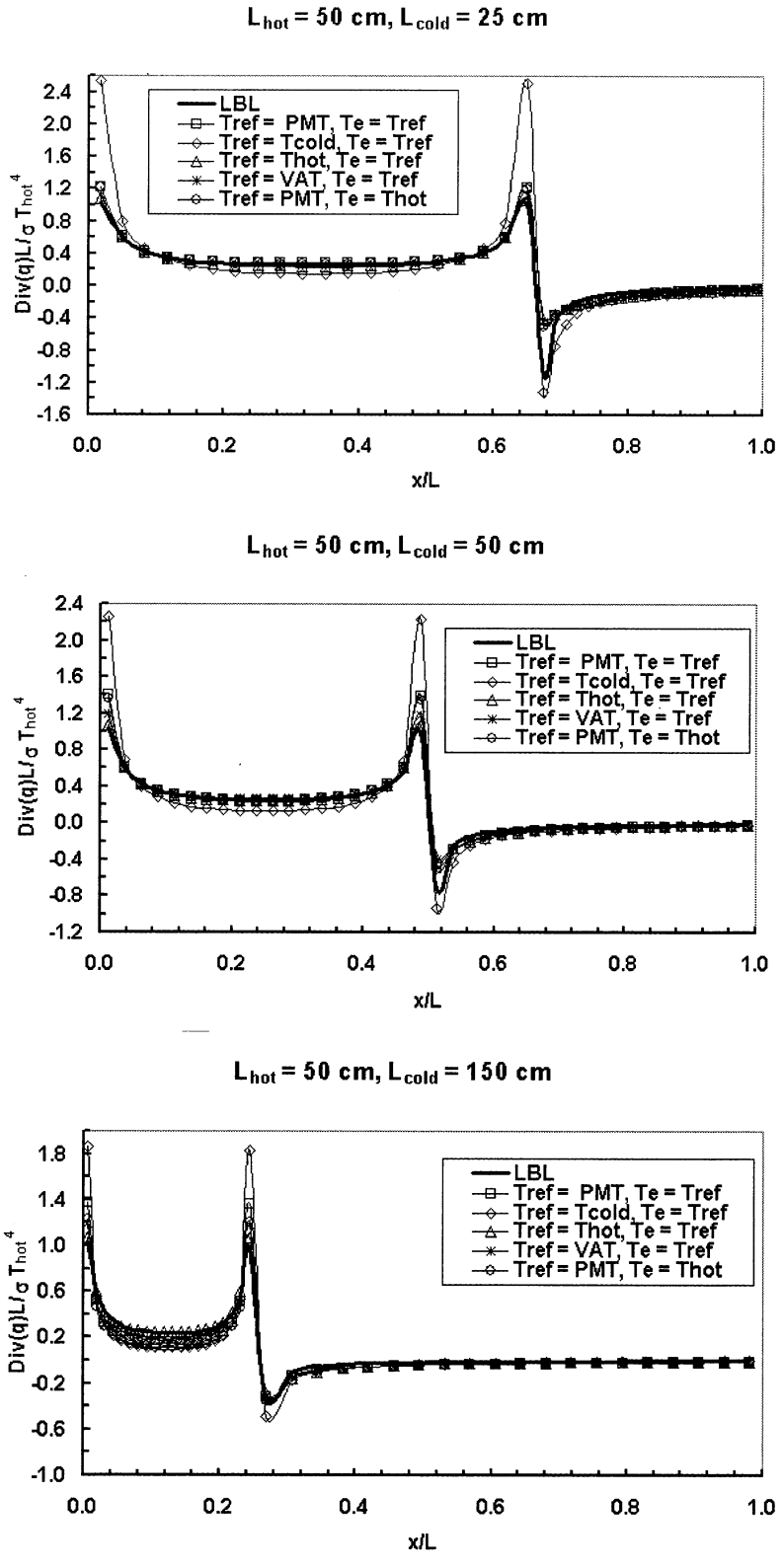


Fig. 9. Comparison of FSCK model with line-by-line (LBL) calculations for various cold layer thickness. The quantity, $L$, is the sum of the thicknesses of the hot and cold layers.

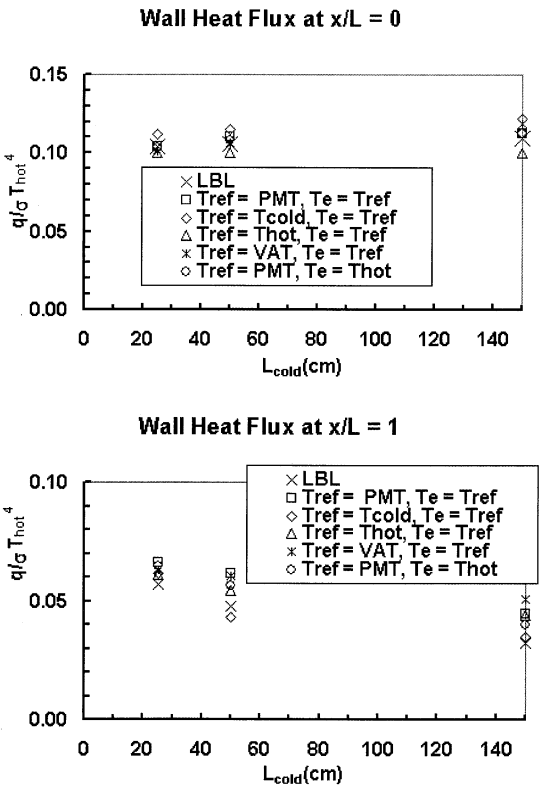


Fig. 10. Wall heat fluxes computed using the FSCK model with different scaling techniques.

$$(\kappa_p T^4)_{ref} = \frac{1}{V}\int_v \kappa_p T^4 dV \tag{25}$$

is more appropriate. Both of these options were examined. Their studies also showed that if the temperature at which the Planck function is evaluated in Eq. 23 is the average emission temperature of the domain, and the absorption coefficient is evaluated at the Planck-mean temperature, the scaling is even more accurate. This is consistent with the physical argument that if $T_{ref} = T_{emission}$ in Eq. 23, the emission from the hot layer is treated more accurately, while using the Planck mean temperature for the absorption coefficient implies that absorption within the cold layer is treated accurately. In principle, it is possible to use separate temperatures for evaluating the absorption coefficient and the Planck function in scaling Eq. 23. This, however, poses additional problems in terms of creating database for the scaling function. It was stated in an earlier section, that currently 129,600 cases need to be evaluated to construct the database for each gas. If the emission temperature is considered a separate independent variable, it would result in 129,600 $\times$ 18 cases, leading to 20 $\times$ 18 days of CPU, which is prohibitive. In light of these observations, this particular scaling technique was deemed impractical for general use. For the problem under consideration, the emission-averaged temperature happens to be very close to 1500 K, that is, the hot layer temperature. In other words, using 1500 K to evaluate the Planck function in Eq. 23 is equivalent to using $T_{emission}$. Figure 9 clearly shows that for $T_{ref} = T_{emission} = T_{hot}$ the results are quite accurate (denoted by triangles) for the hot layer. However, Fig. 10 shows that the heat fluxes on the wall next to the cold layer (x/L = 1) are not so accurate with this approach. The heat fluxes on the same wall are more accurate with the hybrid model (denoted by circles), which uses two independent temperatures for scaling. It is also evident that except for the case where $T_{ref} = T_{cold}$, all other choices of reference temperature produce fairly accurate results. In light of the fact that a 1000 K jump in temperature is quite challenging for scaling, the results lend tremendous credibility to the FSCK model for inhomogeneous temperature fields.

The FSCK model was next validated for a two-dimensional (2D) axisymmetric geometry involving several different boundary temperatures and with temperature jumps as high as 1500 K. The geometry, boundary conditions, and operating parameters for this 2D case are depicted in Fig. 11. In this simulation, the emissivity at all walls was set to 0.5, and gray isotropic scattering was turned on, with a scattering coefficient of 1 $m^{-1}$. The gas in the domain consists of 10% $CO_2$ (by mole) and 90% $N_2$ (assumed non-participating). The divergence of heat flux at the three plotting locations for the three simulations are shown in Fig. 12. In this case too, it is seen that $T_{ref} = T_{emission} = T_{hot}$ accurately predicts the divergence in the hot regions but underpredicts the divergence in the colder regions (x = 0.825). In colder regions, more accurate results are produced either by setting the reference temperature as the Planck-mean temperature or by setting it equal to the volume-averaged temperature. For this particu-

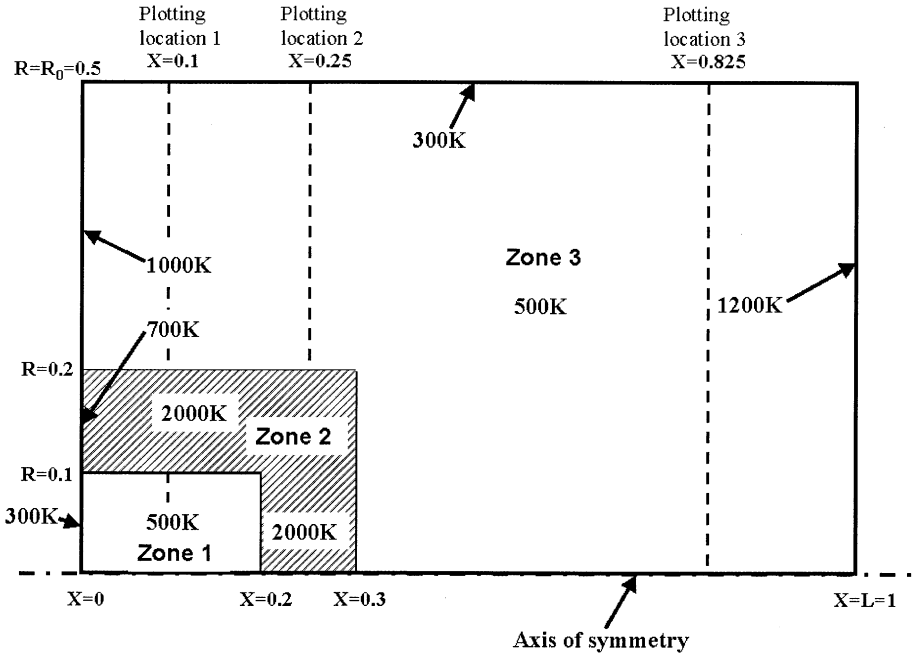


Fig. 11. Geometry, boundary conditions, and operating parameters for 2D axisymmetric test case.

lar case, the volume of the cold region is much larger than the volume of the hot region, and the Planck mean temperature is only about 714 K. Thus, the scaling works well for the cold region if the reference temperature is close to 500 K. The results also prove the validity of the model for gray walls and gray scattering. The conclusion to be drawn from these results is that the predictions are very accurate if the Planck-weighted temperature of the entire computational domain is chosen as the reference temperature, and the emission-weighted temperature is used for computation of the Planck function in Eq. 23. In practice, it is prohibitively expensive to generate the database with two different temperatures, and the best choice is to use the emission-weighted temperature as the reference temperature as well as to compute the Planck function in Eq. 23.

The CPU requirements for performing these calculations need to be mentioned at this point. The LBL calculations, involving about a million bands, requires about 2 days of CPU on an Intel Pentium III 733 MHz processor. This is for the 2D case described above with just 144 cells. In comparison, the FSCK calculations with 8 quadrature points, requires only about 35 seconds of CPU. Of course, the use of the FSCK model requires generation of databases, but this is a one-time affair, and once a database is generated, it can be used for all cases. In fact, plans are underway to publish the databases that we have generated in the open literature, so that future researchers do not have to regenerate these data, but can use the data directly.

### Combined Concentration and Temperature Inhomogeneities

For combustion applications, for which the current model is intended, it is of utmost importance to treat concentration variations along the radiation path. The absorption coefficient of a mixture of gases is approximately linearly proportional to the partial pressures of the constituents:

$$\kappa \approx \sum_i \kappa_i p_i \tag{27}$$

where $\kappa_i$ is the pressure-based absorption coefficient of species $i$, and $p_i$ their partial pressures. This, however, does not apply to reordered $k$-distributions. For such a case, the $k$-distribution changes for each mole-fraction

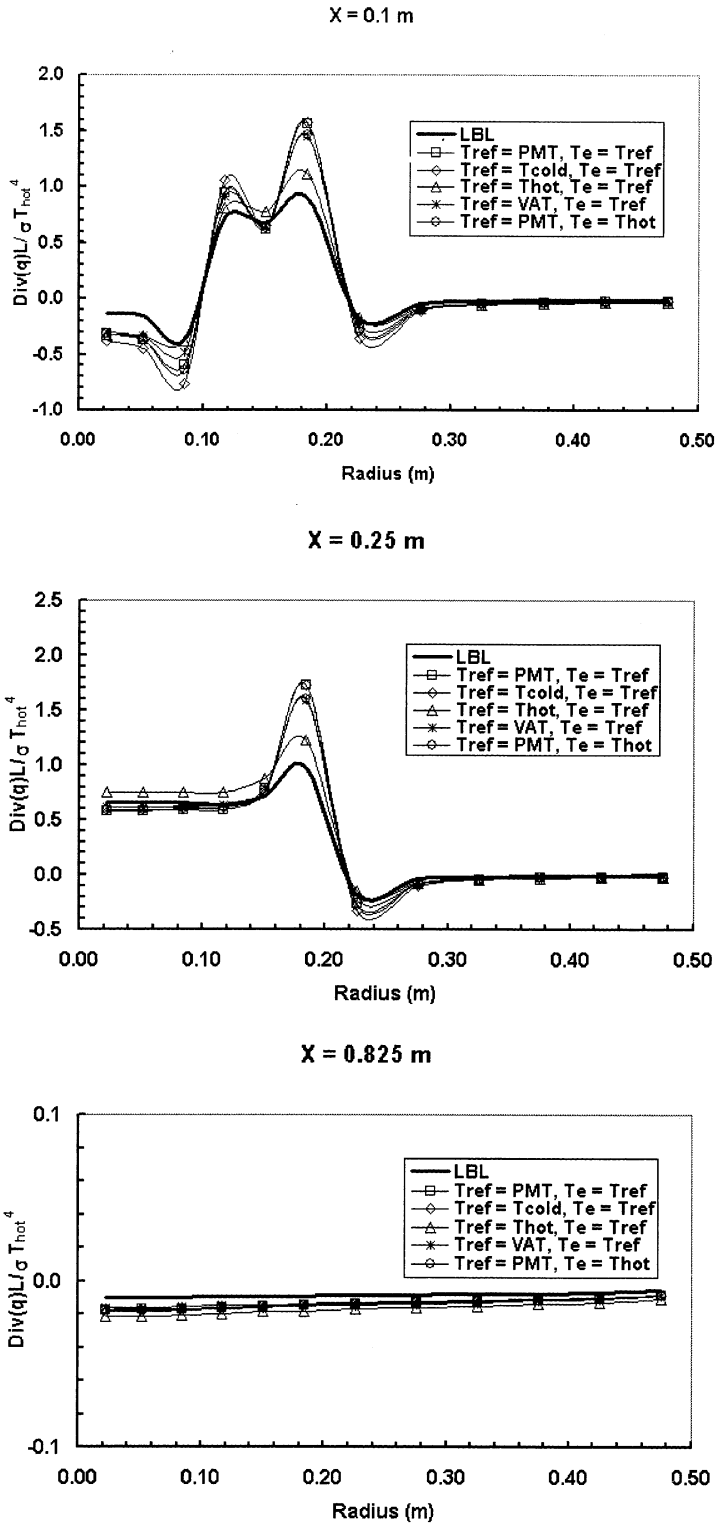


Fig. 12. Comparison of FSCK results with LBL results for 2D axisymmetric case with gray walls (emissivity = 0.5) and isotropic scattering (scattering coefficient = 1 $m^{-1}$)

**TABLE 2**

Composition of Various Spatial Zones for the Two Test Cases with Combined Temperature and Concentration Inhomogeneities

| | Case 1 (Uniform $CO_2/H_2O$ ratio) | | | Case 2 (Non-uniform $CO_2/H_2O$ ratio) | | |
|---|---|---|---|---|---|---|
| | T(K) | $CO_2$ (% mole) | $H_2O$ (% mole) | T(K) | $CO_2$ (% mole) | $H_2O$ (% mole) |
| Zone 1 | 500 | 5 | 10 | 500 | 30 | 10 |
| Zone 2 | 2000 | 10 | 20 | 2000 | 20 | 20 |
| Zone 3 | 500 | 15 | 30 | 500 | 10 | 30 |

combination, and the relationship between *k*-distributions at various concentrations cannot be described adequately by a linear scaling law.

To study the effect of scaling on non-uniform composition fields, we concocted two separate problems. The geometry for both cases is the same as that shown schematically in Fig. 11. The two cases are different by virtue of having constant versus non-constant $CO_2/H_2O$ ratio. The exact composition of the mixtures contained within the three zones for the two cases are tabulated in Table 2. It is worth noting that both cases have strong discontinuities in both temperature and concentrations.

Calculations were performed for both cases using the FSCK model with various strategies for scaling. The results for the uniform $CO_2/H_2O$ ratio case are shown in Fig. 13. Two different reference concentration fields were chosen. The first of these was that corresponding to that of the large outer cold region (Zone 3). The second of these was that corresponding to the middle hot layer (Zone 2). Interestingly enough, the results produced by both of these reference conditions is identical (triangles and circles). If the ratio of $CO_2/H_2O$ is constant, the resulting *k*-distributions at the two reference states have identical profiles, except that they get scaled by a constant factor. For such a scenario, the resultant scaling function is simply a mole-fraction-weighted sum of the individual scaling functions.

When the concentrations of $CO_2$ and $H_2O$ are varied independently, resulting in non-constant $CO_2/H_2O$ ratio, the *k*-distributions for the two reference states may be vastly different, and lead to different results (Fig. 14). For such cases, the resultant scaling function is not a mole fraction weighted sum of the individual scaling functions. For a full-scale combustion application, the reference concentration is expected to change with iteration. As long as the ratio of the mole fractions of the constituent species remain constant, the scaling as applied to the FSCK model is linear, and the results are going to be independent of the reference mole fractions. This is a scenario, which is likely to happen in cases where single-step kinetics is used. For example, for a single step propane-air reaction to $CO_2+H_2O$, the $CO_2/H_2O$ ratio will always be 3:4, although the actual magnitude of the mole fractions may vary from problem to problem and iteration to iteration. If multi-step kinetics is used, the ratio will no longer remain constant because of the production of intermediate species, and the linear scaling argument will be violated. Also, if the fuel is treated as a participating gas, its concentration variation with space is completely uncorrelated with the concentration variation of either $CO_2$ or $H_2O$, that is, the concentration of fuel is high wherever the concentration of $CO_2$ and $H_2O$ is low and vice versa. In such a case, the fuel to $CO_2$ and/or $H_2O$ ratio is guaranteed to be non-constant. Despite this shortcoming of the FSCK model, the results produced even for the case of non-uniform $CO_2/H_2O$ ratio are quite accurate in most cases.

## Demonstration for Full-Scale Combustor

In the validation studies presented in the preceding section, the temperature and/or concentration fields were fixed, and not allowed to change. This was mainly done because LBL calculations are prohibitive for changing conditions because solution of the RTE itself takes a few days of CPU. For a full-scale combustion problem, the temperature and concentration fields will change with every iteration, and LBL

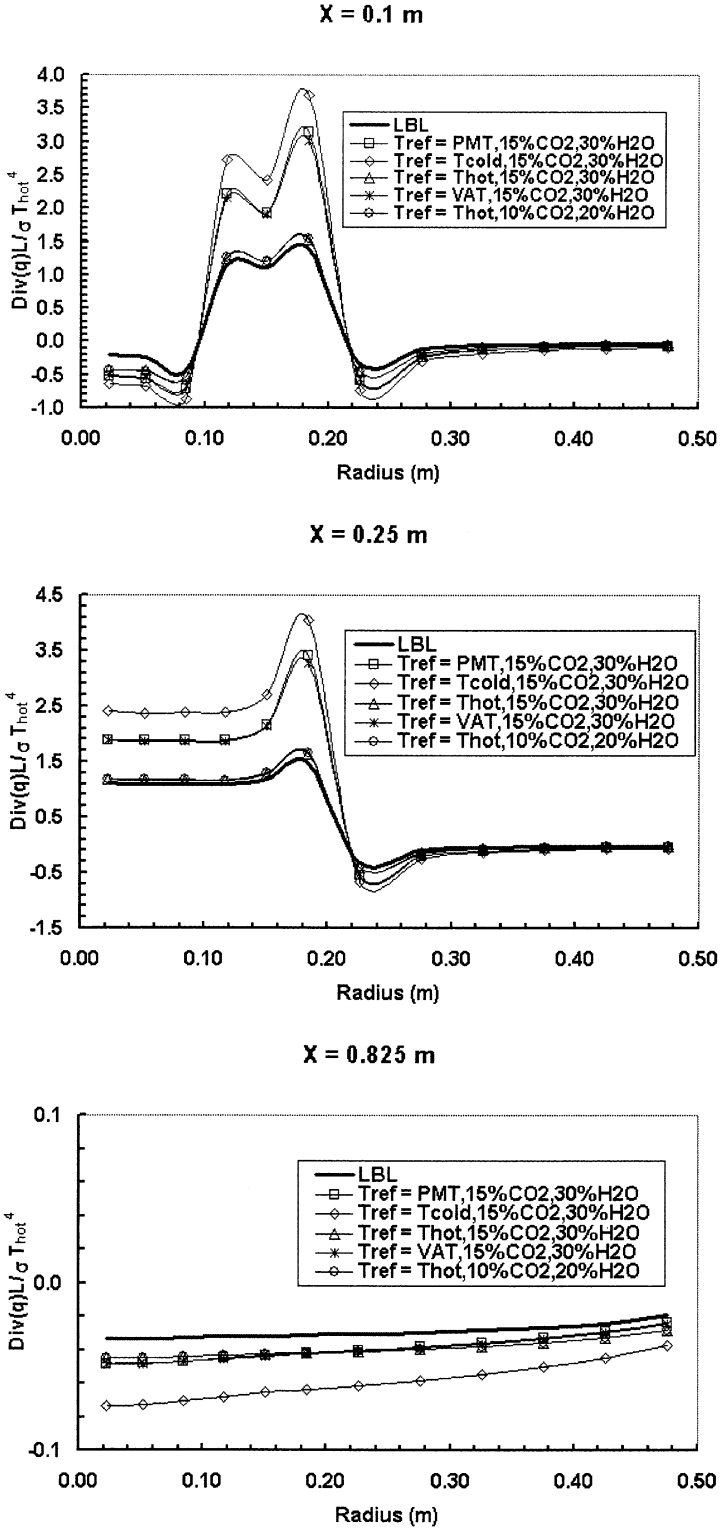


Fig. 13. Comparison of FSCK model with LBL calculations for uniform $CO_2/H_2O$ ratio

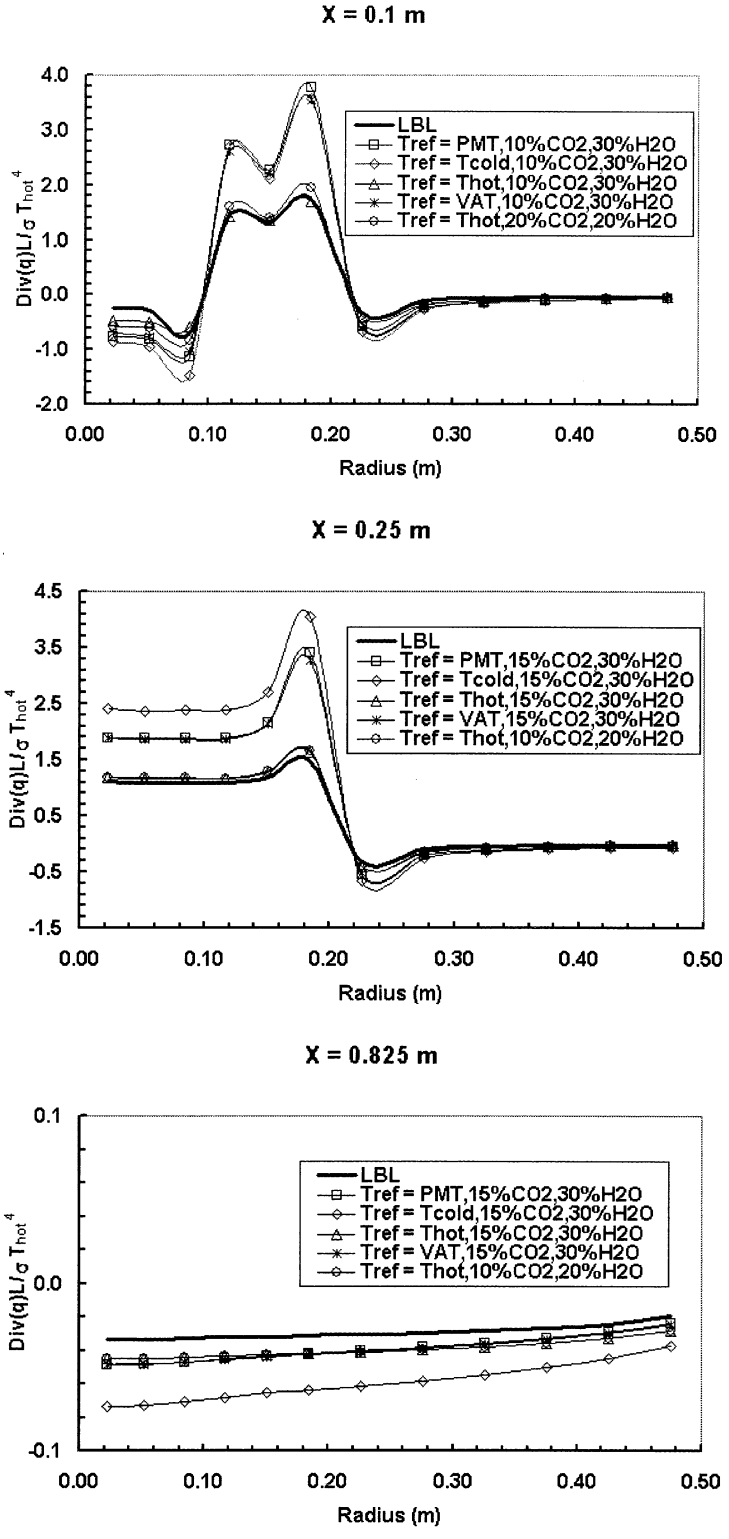


Fig. 14. Comparison of FSCK model with LBL calculations for non-uniform $CO_2/H_2O$ ratio.

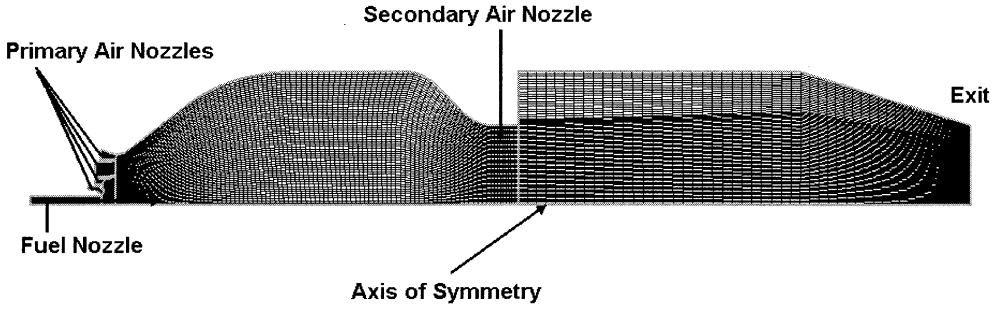


Fig. 15. Geometry and grid for axisymmetric combustor used for demonstrating the FSCK model.

calculations cannot be performed for such a case. Furthermore, each cell will have a different temperature and concentration value, and it is not possible to store that many absorption coefficient arrays in run-time memory. Thus, LBL calculations are prohibitive from a memory perspective, as well. The FSCK code, however, was designed in a manner such that it accounts for changing reference conditions. This is evident in the solution flowchart depicted in Fig. 5, where it is clearly shown that the reference states are recomputed at each iteration of the global solution loop, and the corresponding *k*-distributions, scaling functions and base functions are simply extracted from the database by linear interpolation.

The combustion case undertaken to demonstrate the feasibility of using the FSCK model for real-life combustion applications is discussed next. For simplicity, we considered an axisymmetric version (Fig. 15) of the actual three-dimensional combustor. The combustor has a single fuel nozzle surrounded by four independent air nozzles. There is a secondary air inlet along the annulus, halfway down the length of the combustor to supply excess air. For the current study, we considered combustion of propane in air. The flow rates were adjusted so that the propane fuel undergoes complete combustion, and no excess propane exits the combustor (lean conditions). In order to keep the $CO_2/H_2O$ ratio constant, a single-step global finite-rate reaction was used: $C_3H_8+5O_2 \Rightarrow 3CO_2+4H_2O$. The reaction rate constants were taken from Westbrook and Dryer [34]. The inlet streams were injected at 923 K. The external walls of the combustor were cooled using an external heat transfer boundary condition including both convective as well as radiative losses to a 300 K ambient. JANNAF coefficients were used to compute species thermodynamic properties. The RNG k-$\epsilon$ model, which is a standard option in CFD-ACE+, was used to treat turbulence. Turbulence-chemistry and turbulence-radiation interactions were neglected. Because the HITEMP database is currently limited to $CO_2$ and $H_2O$ only, we also assumed that propane is non-participating. Furthermore, for temperatures above 2000 K, the data for 2000 K was used. This was done mainly because HITEMP data is questionable beyond 2000 K [35,36], and therefore, our database has an upper cutoff of 2000 K. We did not see any benefit of trying to compute such data for this demonstration problem only.

First, a simulation was performed for this geometry without turning on radiation. Next, the Planck-mean absorption coefficient, defined by

$$\kappa_p = \int_0^\infty I_{b\eta}\kappa_\eta d\eta \Big/ \int_0^\infty I_{b\eta} d\eta \tag{28}$$

was computed for $CO_2$ and $H_2O$ at 100 K interval from 300 K to 2000 K. This was tabulated, and Eq. 27 was employed to calculate the gray Planck-mean absorption coefficient at any given temperature and partial pressure after linear interpolation within this table. The next simulation used this gray spatially varying Planck-mean absorption coefficient for radiation calculations. This approach is employed routinely within the combustion community for simplistic radiation

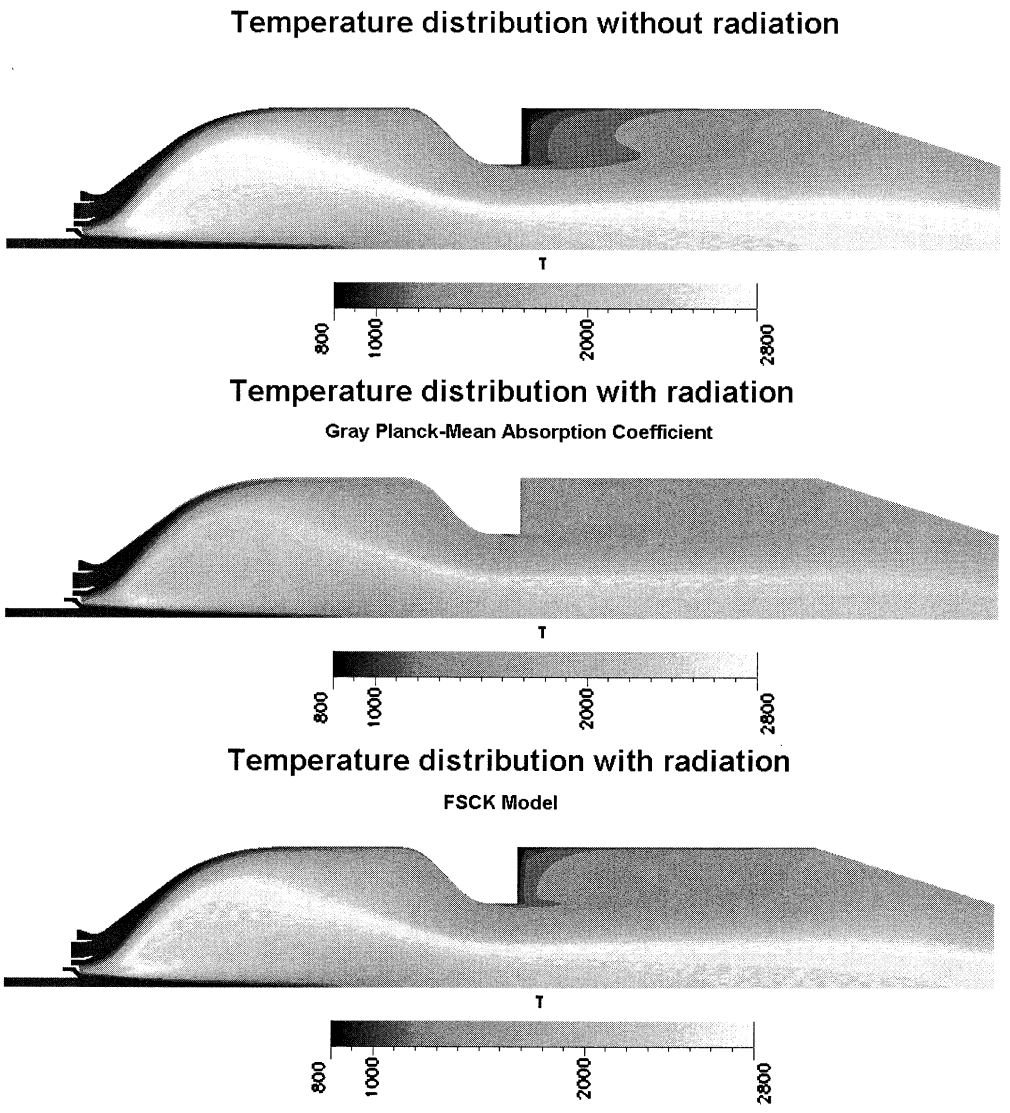


Fig. 16. Steady state temperature profiles for propane-air combustion without radiation and using two different radiation models.

calculations, and more or less represents the state-of-the-art when it comes to calculation of radiation in combustion systems [37]. Finally, the FSCK model was used to compute radiation fluxes. The reference condition chosen was the Planck-mean temperature, which was automatically recomputed at each iteration of the global solution loop. The reference concentration was taken to be the volumetric average, which was also recomputed. The temperature profiles obtained for the three cases are shown in Fig. 16. Obviously, without radiation, the flame temperature is severely overpredicted. With the gray Planck-mean absorption coefficient, the absorption by colder regions is overpredicted and the emission by hotter regions is also overpredicted resulting in a much more uniform temperature distribution. With the FSCK model, the sharp flame structure is retained, and the flame is colder by about 200 K compared to the case without radiation.

The CPU required to simulate the case with the FSCK model was only 25% more than the

CPU required for the case without radiation. The fractional increase in CPU is expected to be significantly lower for cases with multi-step chemistry involving many species. The total CPU required for three order of magnitude convergence of this problem involving 11,410 cells was about 210 min on a 733 MHz Intel Pentium III processor.

## SUMMARY AND CONCLUSIONS

The full spectrum correlated $k$-distribution approach is a powerful approach to modeling nongray radiation in combustion gases. Its accuracy is comparable to exact solutions of the RTE for homogeneous gas layers. For inhomogeneous gas layers with strong discontinuities in both temperature and concentrations, its accuracy is limited by the scaling approximation. Several different full-spectrum scaling techniques were investigated, and it was found that a reference temperature equal to the emission-weighted temperature of the domain, and a reference concentration equal to the volume-averaged concentration yields best results. For all cases considered under this study, results were always within 20% of LBL answers. Global spectrum approaches, such as the FSCK approach and the SLW approach have the disadvantage that they are sensitive to the choice of reference conditions when it comes to treatment of radiation in inhomogeneous media. One alternative is to use local spectrum approaches, which are far more computationally expensive, but produce accurate results independent of the choice of reference conditions, as demonstrated recently by Solovjov and Webb [38].

When used in conjunction with the Discrete Ordinates Method, the FSCK model can prove to be a powerful tool for computing radiative fluxes within full-scale combustors involving coupled fluid flow, heat transfer, and chemistry in complex geometries. It was found that the additional CPU requirement (to compute radiative fluxes) is less than 25% for a full-scale combustion problem involving 5 species, and is expected to be significantly lower with increase in the number of species.

*The support of the National Science Foundation through an SBIR Phase I grant (Contract # DMI 0060286, Program Officer: Cheryl Albus) is gratefully acknowledged.*

## REFERENCES

1. Elsasser, W. M., *Harvard Meterol.* 6:107 (1942).
2. Ludwig, C. B., Malkmus, W., Reardon, J. E., and Thompson, J. A., *Handbook of Infrared Radiation from Combustion Gases*, NASA SP-3080, Scientific and Technical Information Office, Washington DC, 1973.
3. Edwards, D. K., *Advances in Heat Transfer* 12:115–193 (1976).
4. Rothman, L. S. et al., 1992, *J. Quant. Spectrosc. Rad. Transfer*, Vol. 48, pp. 469–507.
5. Rothman, L. S. *et al.*, 1998, HAWKS (HITRAN Atmospheric Workstation): 1996 Edition," *J. Quant. Spectrosc. Rad. Transfer*, Vol. 60, pp. 665–710.
6. Lacis, A. A, and Oinas, V., 1991, *Geophys. Res*. Vol. 96, No. D5, pp. 9027–9063.
7. Denison, M. K. and Webb, B. W., *Quant Spectrosc. Rad. Transfer* 50:499–510 (1993).
8. Denison, M. K. and Webb, B. W., *Heat Transfer* 115:1004–1012 (1993).
9. Modest, M. F. and Zhang, H., *Heat Transfer* 124(1): 30–38 (2002).
10. Riviere, P., Soufiani, A., and Taine, J., *J. Quant. Spec. Rad. Transfer* 48(2):187–203 (1992).
11. Pierrot, L., Riviere, P., Soufiani, A., and Taine, J., *J. Quant. Spec. Rad. Transfer* 62:609–624 (1999).
12. Malkmus, W., *J. Opt. Soc. Am*. 57(3):323 (1967).
13. Hartmann, J. M., DeLeon, R. and Taine, J., *J. Quant. Spectrosc. Rad. Transfer* 32(2):119 (1984).
14. Lee, P. Y. C., Hollands, K. G. T. and Raithby, G. D., *J. Heat Transfer* 118(2):394 (1996).
15. Riviere, P., Scutaru, D., Soufiani, A., and Taine, J., *Tenth International Heat Tranafer Conference*, Taylor and Francis, 1994, pp. 129–134
16. Riviere, P., Soufiani, A., and Taine, J., *J. Quant. Spec. Rad. Transfer* 53:335–346 (1995).
17. Modest, M. F., *Heat Transfer* 113(3): 650 (1991).
18. Denison M. K. and Webb, B. W., *Tenth International Heat Transfer Conference*, Taylor & Francis, 1994, pp. 19–24.
19. Denison M. K. and Webb, B. W., *Heat Transfer* 117:359–365 (1995a).
20. Denison M. K. and Webb, B. W., *Heat Transfer* 117:788–792 (1995b).
21. Solovjov, V. P. and Webb, B. W., *J. Quant. Spectrosc. Rad. Transfer* 65:655–672 (2000).
22. Arking, A. and Grossman, K., *J. Atmosphe. Sci.* 29: 937–949 (1972).
23. Goody, R., West, R., Chen, L., and Crisp, D., *J. Quant. Spectrosc. Rad. Transfer* 42(6):539 (1989).
24. Tang, K. C. and Brewster, M. Q., *J. Heat Transfer* 116:980 (1994).
25. Zhang, H. and Modest, M. F., Proceedings of the

ICHMT Third International Symposium on Radiative Heat Transfer, 2001, Antalya, Turkey.
26. Modest, M. F., *Radiative Heat Transfer*, McGraw Hill, New York, 1993.
27. Modest, M. F., *Heat Transfer* 112: 819–821 (1990).
28. Fiveland, W. and Jamaluddin, A., *Thermophysics and Heat Transfer* 5(3):335–339 (1991).
29. Chai, J. C., Lee, H. S. and Patankar, S. V., *Journal of Thermophysics and Heat Transfer* 8:419–425 (1994).
30. Lockwood, F. C., and Shah, N. G., *Eighteenth Symposium (International) on Combustion: The Combustion Institute*, Pittsburg, 1981, pp. 1405–1409.
31. Modest, M. F., *Numerical Heat Transfer, Part B* 22(3): 273–284 (1992).
32. Vaidya, N., Multi-dimensional Simulation of Radiation Using An Unstructured Finite Volume Method, *AIAA Paper number 98–0856*, 1998.
33. Abramowitz, M. and Stegun, I. A, Eds., *Handbook of Mathematical Functions*, Dover Publications, New York, 1965.
34. Westbrook, C. K. and Dryer, F. L., *Combust. Sci. Technol.* 27:31–43 (1981).
35. Taine, J. and Soufiani, A., *Gas IR Radiative Properties: From Spectroscopic Data to Approximate Models*, Vol. 33, Academic Press, New York, 1999.
36. Modest, M. F. and Bharadwaj, S., *Proceedings of the ICHMT third International Symposium on Radiative Heat Transfer*, Antalya, Turkey, 2001.
37. DesJardin, P. E. and Frankel, S. H., *Proceedings of the Technical Meeting of the Central States Section of the Combustion Institute*, 1998.
38. Solovjov, V. P. and Webb, B. W., *Proceedings of the Third International Symposium on Radiative Transfer*, Eds. Menguc and Selcuk; Begell House, NY, 2001, pp. 177–185.

*Received 21 August 2001; revised 25 January 2002; accepted 10 February 2002.*